Involvement of the exomer complex in the polarized transport of Ena1 required for *Saccharomyces cerevisiae* survival against toxic cations

Carlos Anton[a], Bettina Zanolari[b], Irene Arcones[a], Congwei Wang[b], Jose Miguel Mulet[c], Anne Spang[b,*], and Cesar Roncero[a,*]

[a]Instituto de Biología Funcional y Genómica (IBFG) and Departamento de Microbiología y Genética, CSIC-Universidad de Salamanca, 37007 Salamanca, Spain; [b]Biozentrum, Growth & Development, University of Basel, CH-4056 Basel, Switzerland; [c]Instituto de Biología Molecular y Celular de Plantas, CSIC-Universitat Politécnica de Valencia, 46011 Valencia, Spain

ABSTRACT Exomer is an adaptor complex required for the direct transport of a selected number of cargoes from the *trans*-Golgi network (TGN) to the plasma membrane in *Saccharomyces cerevisiae*. However, exomer mutants are highly sensitive to increased concentrations of alkali metal cations, a situation that remains unexplained by the lack of transport of any known cargoes. Here we identify several *HAL* genes that act as multicopy suppressors of this sensitivity and are connected to the reduced function of the sodium ATPase Ena1. Furthermore, we find that Ena1 is dependent on exomer function. Even though Ena1 can reach the plasma membrane independently of exomer, polarized delivery of Ena1 to the bud requires functional exomer. Moreover, exomer is required for full induction of Ena1 expression after cationic stress by facilitating the plasma membrane recruitment of the molecular machinery involved in Rim101 processing and activation of the RIM101 pathway in response to stress. Both the defective localization and the reduced levels of Ena1 contribute to the sensitivity of exomer mutants to alkali metal cations. Our work thus expands the spectrum of exomer-dependent proteins and provides a link to a more general role of exomer in TGN organization.

INTRODUCTION

Transmembrane proteins are regularly sorted into membrane vesicles for their traffic through the secretory and endocytic pathways by the action of dedicated cargo adaptors (Schekman and Orci, 1996; Bonifacino and Glick, 2004; De Matteis and Luini, 2008). These adaptors not only direct cargo loading but perform additional functions in vesicle biogenesis, including recruitment and the stabi-

lization of other coat components (Bonifacino and Lippincott-Schwartz, 2003; Spang, 2008).

Very limited mechanistic data are available concerning cargo sorting at the *trans*-Golgi network (TGN), one of the most prominent sorting stations in eukaryotic cells, in which cargo is packaged into vesicles destined for the plasma membrane (PM) (Bard and Malhotra, 2006; Bonifacino, 2014). In *Saccharomyces cerevisiae*, such secretory vesicles are the main source of lipids and proteins used to generate the PM of a daughter cell (Drubin and Nelson, 1996). However, the mechanisms involved in the biogenesis of these secretory vesicles, as well as the mechanisms for cargo sorting, have long remained elusive. The analysis of the exomer complex provided some mechanistic understanding of TGN sorting in *S. cerevisiae* (Trautwein *et al.*, 2006; Wang *et al.*, 2006). Exomer serves as a kind of sorting platform at the TGN for the delivery of Chs3 and Fus1 to the PM (Barfield *et al.*, 2009; Trautwein *et al.*, 2006). Both proteins display a characteristic polarized distribution.

Moreover, exomer is well conserved across fungi (Trautwein et al., 2006; Roncero et al., 2016), raising some expectations as to whether exomer could act as a general platform for the sorting of polarized proteins at the TGN in fungi. Unfortunately, such expectations have not been fulfilled as the extensive efforts by several groups have only shown a very limited number of proteins to depend on exomer for PM localization. These include Chs3 (Santos and Snyder, 1997; Trautwein et al., 2006), Fus1 (Barfield et al., 2009), and the more recently described Pin2 (Ritz et al., 2014), all of which are transmembrane (TM) proteins with polarized distribution. In contrast, we have advanced significantly in the understanding of the mechanistic aspects of the exomer complex itself. This complex is assembled at the TGN as a heterotetramer, consisting of two copies of the scaffold protein Chs5 and any two members of four paralogous proteins known as ChAPs (Chs5 and Arf1 binding proteins: Chs6, Bud7, Bch1, and Bch2) (Paczkowski et al., 2012; Paczkowski and Fromme, 2014; Huranova et al., 2016). The ChAPs and Chs5 bind to the Arf1 GTPase and help to remodel membranes, a process that is required for vesicle formation in vitro (Paczkowski and Fromme, 2014). Interestingly, not all ChAPs are equally effective in assembling the exomer complex. Bch1 and Bud7 have been proposed to be the most effective in triggering membrane remodeling because of a characteristic hydrophobic element in their sequences that is not present in Chs6 and Bch2 (Paczkowski and Fromme, 2014). Accordingly, Bch1 and Bud7 have been independently shown to be more efficient in the stabilization of exomer complexes (Huranova et al., 2016).

Furthermore, ChAPs subunits have been proposed to determine cargo specificity by their direct interaction with the cytosolic tails of cargo proteins, a process in which Chs6 and Bch2 are the most effective (Huranova et al., 2016). However, the direct interaction between the ChAPs and cargo has only been well documented for Chs6, which has been shown to interact with two different domains of its distinct cargo, Chs3. Deletion of specific N- and C-terminal cytosolic regions of Chs3 abolished exomer recognition and blocked Chs3 transport from the TGN (Rockenbauch et al., 2012; Weiskoff and Fromme, 2014). Also, the chs6Δ mutant shares with chs5Δ all the phenotypes linked to the reduced levels of chitin brought about by Chs3 TGN sequestration (reviewed in Roncero [2002]) but none of the other exomer-related phenotypes.

As pointed out above, the number of exomer cargoes is small, and the known cargoes are rather different in terms of primary sequence, number of transmembrane domains (ranging from 1 to 8, based on bioinformatics analysis), and topology (type I and II TM proteins), making it difficult to understand the biological functions of exomer. However, all of the cargoes are localized in a polarized manner and are completely retained at the TGN in the absence of exomer. Interestingly, their transit to the PM is always restored in the absence of the AP-1 complex (Valdivia et al., 2002; Barfield et al., 2009; Ritz et al., 2014), suggesting that it is their interaction with the AP-1 complex that makes them dependent on exomer for their arrival to the PM. This in fact has been shown in detail for Chs3, in which a specific N-terminal cytosolic region is required for its interaction with AP-1 (Starr et al., 2012). In the absence of this domain, Chs3 still reaches the PM even in the absence of exomer (Starr et al., 2012; Sacristan et al., 2013). Similar data have been reported for Pin2 (Ritz et al., 2014).

An intriguing unresolved issue regarding exomer function is the fact that exomer deficient mutants are highly sensitive to lithium, sodium, ammonium, or hygromycin (Trautwein et al., 2006; Fell et al., 2011; Ritz et al., 2014). These phenotypes cannot be explained by defective transport of any of the previously described exomer cargoes, including Pin2, which is rapidly endocytosed under hyperosmotic condition but whose deletion displays no increased Li$^+$ sensitivity (Ritz et al., 2014). All of the above substances are cationic molecules whose intracellular toxicity is prevented by either reducing their uptake or increasing their efflux through the regulation of several PM transporters. Alkali-metal cation uptake depends mostly on the activity of Trk1/2 potassium uniporters, while efflux relies on the activity of the potassium channel Tok1, the cation-proton antiporter Nha1, and the cation ATPase Ena1 (review in Ariño et al., 2010). The regulation of such transporters is complex, and positive and negative regulators have been described. Several HAL (for halotolerance) gene products have been shown to act as positive regulators of these transporters, including Hal1 (Rios et al., 1997), Hal3 (de Nadal et al., 1998), and the Ser/Thr kinases Hal4 and Hal5 (Mulet et al., 1999). In contrast, Hal2 is involved in halotolerance as a direct target of sodium toxicity (Murguia et al., 1996). The activity of the protein phosphatases Ppz1/2 negatively regulates the potassium uptake mediated by Trk1/2, thus being negative regulators of halotolerance (Yenush et al., 2002). Moreover, in the regulation of such transporters several signal transduction pathways also converge, including the calcineurin- and RIM101-dependent responses (Ariño et al., 2010).
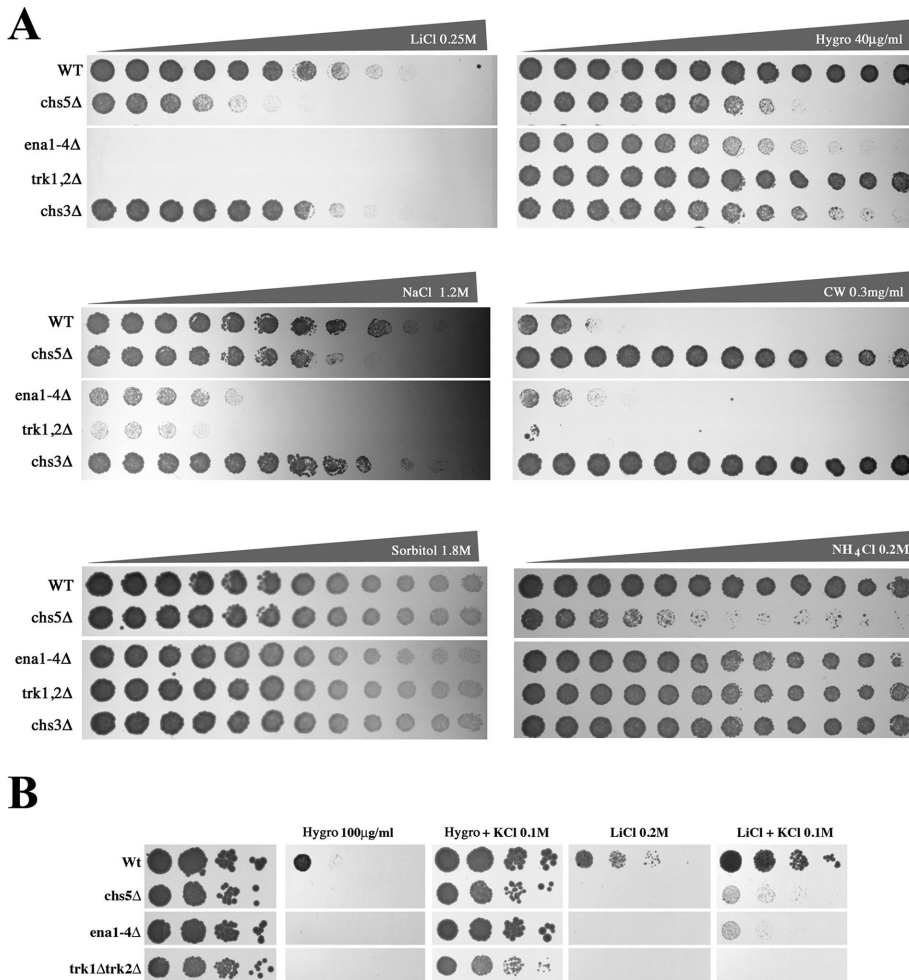
In this paper, we systematically addressed the hypersensitivity of the exomer mutant chs5Δ to cationic molecules by characterizing its phenotypes in detail and by identifying multicopy suppressors of cation sensitivity. Our results link the cation sensitivity observed in exomer mutants to defects in Ena1 ATPase function. Exomer appears to be involved in Ena1 function through two separate mechanisms: first, by controlling Ena1 expression through the RIM101 pathway and, second, by facilitating polarized Ena1 localization in the bud. Our results thus identify Ena1 as a novel exomer cargo and uncover new roles for the exomer complex.

RESULTS

Exomer mutants exhibit sensitivity toward cations and positively charged molecules

To understand the basis of the sensitivity of exomer mutants toward cationic molecules, we first compared the phenotypes of an exomer mutant to those with deletions in cationic transporters with similar hypersensitivities to cations (Figure 1), such as Trk1/2 and Ena1, major facilitators of K$^+$ transport across the PM in yeast (Ariño et al., 2010). We did not include Pma1 mutants because defects in the function of this ATPase have been linked to moderate resistance to cationic compounds (Perlin et al., 1988). Therefore, a direct relationship between exomer and the function of Pma1 is unlikely. Trk1/2 have been reported to be the major K$^+$ channel, while through genetic studies it became clear that the family Ena Na$^+$ transporters is also involved in K$^+$ homeostasis (Ariño et al., 2010). Since Ena transporters are present in clusters, are highly conserved, and might have at least partially redundant functions, we used a mutant in which the cluster containing the four ENA genes was deleted (ena1-4Δ) (Yenush et al., 2002). The quadruple ena1-4Δ and the double trk1/2Δ mutants were both sensitive to Li$^+$ and Na$^+$, but only the ena1-4Δ mutant was sensitive to hygromycin (Figure 1A); thus the chs5Δ phenotypes were more similar to those of the ena1-4Δ mutant. None of the ion transporter mutants showed resistance to calcofluor or sensitivity to NH$_4$$^+$ (Figure 1A), the other classical phenotypes associated with exomer mutants (Trautwein et al., 2006) or were sensitive to high osmolarity.

On the basis of the similarity of phenotypes, we next tested the localization of several major PM cation transporters in an exomer mutant to determine whether the transport of any of these proteins

FIGURE 1: Comparative sensitivity between mutant strains defective on exomer or different cation transporters. (A) Growth of different yeast strains on YEPD plates supplemented with increased concentrations of the indicated compounds. Gradient plates from 0 to the specified maximum concentration were made as described under *Materials and Methods*. (B) Sensitivity of the indicated strains to hygromycin or Li$^+$ in the absence or presence of 0.1 M KCl. Note the full suppression of hygromycin sensitivity on KCl-containing plates compared with the limited effect on Li$^+$ sensitivity.

sensitivity of exomer mutants and the ion transporter mutants to hygromycin, but not to Li$^+$, was abolished by high K$^+$ concentrations in the medium (Figure 1B), suggesting that the K$^+$ and Li$^+$ growth defects were not directly correlated. Taken together, our data so far indicate an involvement of exomer in cation homeostasis, which might be connected to the functionality of ion channels potentially through an altered function of cation extrusion.

Upregulation of halotolerance suppressed *chs5Δ* cationic sensitivity through upregulation of Ena1 ATPase

To gain a better understanding of the process, we searched for multicopy suppressors of the Li$^+$ sensitivity of the *chs5Δ* mutant by selecting colonies that were able to grow on plates containing 0.2 M Li$^+$. After eliminating *CHS5*-containing plasmids, subcloning revealed both *HAL1* and *MTC1* as suppressors. The Maintenance of Telomer Capping gene *(MTC1)* is a poorly characterized gene whose overexpression was reported be lethal (Sopko *et al.*, 2006), which explains why the *MTC1* overexpression rescue potential of *chs5Δ* on 0.2 M Li$^+$ was variable. Therefore, we focused our efforts on the other suppressor, *HAL1*. *HAL1* acted as a bona fide suppressor, since its overexpression restored growth of the *chs5Δ* mutant at 0.15 M Li$^+$ and 0.8 M Na$^+$ (Figure 3A) but not on high NH$_4$$^+$. Hal1 provides halotolerance by decreasing cellular Na$^+$ via upregulation of Ena1 and by increasing K$^+$ through decreasing efflux (Rios *et al.*, 1997). Moreover, other *HAL* genes are involved in either transcriptional activation of *ENA1* or the regulation of Trk1/2 activity (Mulet *et al.*, 1999; Yenush *et al.*, 2002). Consequently, we asked whether overexpression of those *HAL* genes could also rescue the *chs5Δ* cation sensitivity. Overexpression of *HAL3*, 4 and 5 also fully restored the growth of the *chs5Δ* mutant on high Li$^+$ and Na$^+$ plates, but only overexpression of *HAL3* significantly improved growth on NH$_4$$^+$-supplemented media (Figure 3B). Hal3 is a negative regulator of the protein phosphatase Ppz1, which in turn is a negative regulator of Trk1/2 activity (Yenush *et al.*, 2002), while *HAL4* and *HAL5* encode for kinases acting as activators of Trk1/2 (Mulet *et al.*, 1999). Consistently, deletion of *PPZ1* improved growth of *chs5Δ* on Li$^+$ and Na$^+$ plates (Figure 3C). However, in contrast, overexpression of *HAL2*, a bisphosphate-3'-nucleotidase (Murguia *et al.*, 1996), had no effect on *chs5Δ* mutant phenotypes despite its expression levels being higher than that of *HAL5* (see Supplemental Figure S1). Taken together, our results indicate that overexpression of positive regulators of ion transporters improves the tolerance of *chs5Δ* toward high concentrations of cations, in particular alkali metals.

was dependent on exomer. Trk1, Nha1, or Qdr2 localization was not affected in exomer mutants (Figure 2A). Ena1-GFP was barely detectable under normal growth conditions due to low expression levels, and therefore its localization was also assessed at pH 7.0 (Figure 2A, right panel). Again, Ena1-GFP efficiently reached the PM in both strains, and its localization appeared indistinguishable from that in wild type and the *chs5Δ* mutant. Therefore, our results did not indicate a direct link between Li$^+$/Na$^+$ sensitivity and defective localization of any of the major pumps involved in cation transport.

Finally, we determined Rb$^+$ uptake as an indirect measurement of K$^+$ transport and the cellular K$^+$ content. In exomer-deficient mutants, Rb$^+$ uptake was significantly impaired and comparable to the level of the *trk1/2Δ* K$^+$ transporter strain (Figure 2B). Interestingly, *chs5Δ* was more defective than the ChAPsΔ strain, indicating both a ChAPs-dependent and -independent function of Chs5 in this process. Likewise, a reduction of the intracellular K$^+$ content was observed in all mutants to the same extent as that observed in *trk1/2Δ* strains (Figure 2C). While the single ChAP deletion *bch1Δ* displayed a Rb$^+$ uptake activity similar to wild type, the K$^+$ levels were reduced, suggesting an increased K$^+$ efflux in this mutant. Interestingly, the

Given the results mentioned above, we hypothesized that downregulation of cationic transporters might be the cause for the Li$^+$ and Na$^+$ sensitivity of the exomer-deficient mutant *chs5Δ*. If our assumption was correct, then increasing the levels of cation-specific
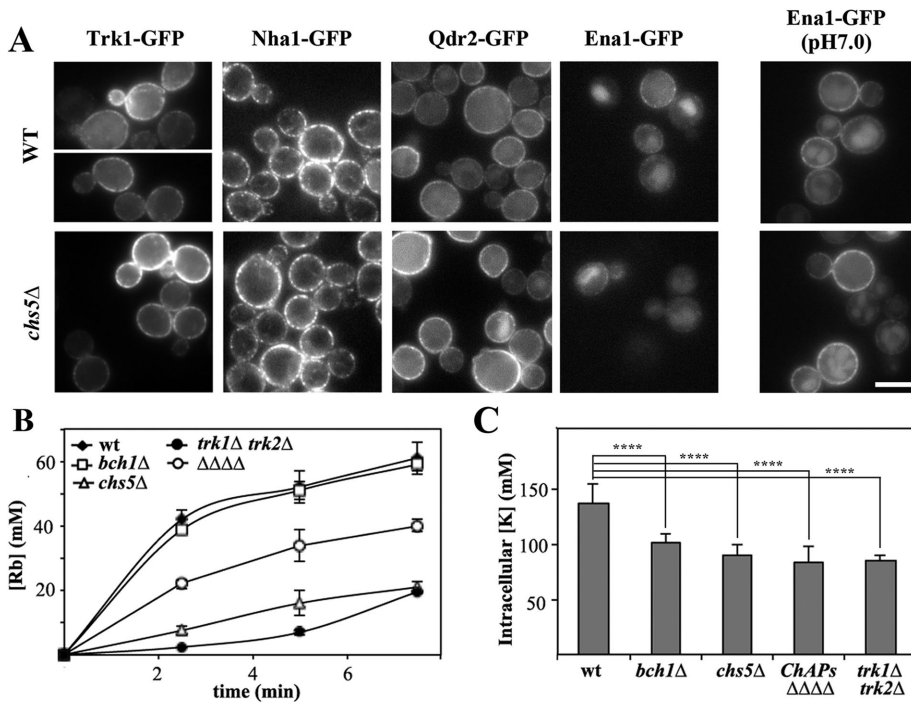
FIGURE 2: The localization of PM transporters in exomer mutants. (A) Localization of different PM transporters in wild-type and *chs5Δ* strains. Proteins were chromosomally appended with the GFP at their C-terminus, except Trk1-GFP, which was expressed from plasmid pRS414. All proteins were visualized in cells growing in nonbuffered SD media except Ena1-GFP, which was also visualized at pH 7.0. Note the similar localization in wild-type and *chs5Δ* strains. (B) Rubidium uptake in the different mutants and (C) intracellular levels of potassium. The strain labeled ΔΔΔΔ corresponds to strain YAS563-16a in which all four ChAPs have been deleted (see Table 1).

permeases should equally increase ion tolerance of *chs5Δ*. Of the six candidates tested (*ENA1, TRK1, KHA1, NHX1, NHA1,* and *QDR2*) only overexpression of *ENA1* and *QDR2* improved growth of *chs5Δ* on Li⁺ or Na⁺-supplemented plates (Figure 4A), and this effect cannot be explained by low expression levels of some of the genes as all genes were well overexpressed (Supplemental Figure S1). Ena1 and Qdr2 are both extrusion pumps. Therefore, the sensitivity of *chs5Δ* to cations is probably linked to a defect in extrusion of the toxic ions rather than to an influx defect. To test this notion, we measured Li⁺ extrusion in both wild-type and *chs5Δ* strains (Figure 4B), resulting in a clearly reduced export of Li⁺ in the *chs5Δ* mutant. In contrast to *ena1-4Δ*, *qdr2Δ* is neither Li⁺ nor Na⁺ sensitive (Ríos et al., 2013). Moreover, Qdr2 was the sole transporter that was also able to rescue the NH₄⁺ sensitivity of *chs5Δ*, reinforcing the idea that NH₄⁺ and alkali metal sensitivity are genetically and physiologically separable. Thus, our analysis so far clearly points to low Ena1 activity at the plasma membrane as the cause for *chs5Δ* sensitivity toward alkali metals. Therefore, we focused our further analysis on Ena1.

## The absence of exomer alters Ena1 expression and intracellular localization

First, we set out to solve a conundrum, since, as shown in Figure 2, we presented evidence that Ena1 localization was independent of an exomer, even though all the genetic evidence contradicted this finding, unless an Ena1-activating cofactor was evoked as a cargo-dependent exomer. Thus, we reassessed Ena1-GFP localization after confirming that the Ena1-GFP construct was functional (Supplemental Figure S2A). *ENA1* expression is under strong transcriptional control (see (Ariño et al., 2010) for a review). Therefore, Ena1-GFP

was barely detected at acidic pH, such as in synthetic defined (SD) medium (Figure 5A); although some cells showed polarized distribution of the protein in the wild type (Figure 5A). Remarkably, Ena1-GFP levels seemed reduced in the *chs5Δ* mutant since fluorescence was barely detectable at the PM of the mutant. Raising the pH of the medium to pH 7.0 for 35 min significantly increased the fluorescence signal and, more importantly, still 50.6% of the wild-type cells showed polarized Ena1 distribution. In contrast, Ena1-GFP levels in the *chs5Δ* mutant remained apparently lower, and the level of polarization was reduced (28.5%) compared with the wild type. Interestingly, maintaining pH 7 for 2 h led to almost complete loss of polarity of Ena1-GFP, and its localization became very similar in both strains. Challenging the cells with Na⁺ reverted the equal Ena1 plasma membrane distribution to a polarized localization in the bud. Even though this effect was observed in both strains, the repolarization was less efficient in *chs5Δ* compared with wild type. We sought an alternative way to analyze the polarization phenotype, which would also be independent of the Ena1-GFP expression levels in wild type and *chs5Δ*. We decided to determine the polarization coefficient given by the mean fluorescence intensity of the plasma membrane in the bud over the one in the mother cell (Figure 5B; see also Supplemental Figure S3A). Our data indicate that not only fewer cells show polarized Ena1-GFP localization in *chs5Δ* at pH 7 for 35 min and on addition of NaCl (Figure 5A) but also that the level of polarization is reduced when compared with wild type (Figure 5B). Therefore, exomer contributes to the polarized localization of Ena1 under acute stress conditions.

The effect of the absence of exomer on Ena1 expression was also confirmed by Western blot. Under noninducing conditions in SD media, Ena1-GFP was undetectable in both wild-type and *chs5Δ* strains (Figure 5C). Raising the pH to 7.0 (Figure 5C) or by directly adding NaCl to the media (see Figure S2C) triggered expression of Ena1 in both wild-type and *chs5Δ* cells, although levels of the protein were always moderately lower in the *chs5Δ* mutant (Figure 5C and Supplemental Figure S2C). The effects of adding NaCl and alkalinization were additive because NaCl treatment after alkalinization of the medium augmented Ena1-GFP levels even further (Figure 5C). Interestingly, in yeast extract peptone dextrose (YEPD) medium Ena1-GFP was detectable in the wild type but not in the *chs5Δ* mutant (Supplemental Figure S2C), confirming the general lower abundance levels of Ena1 in the exomer mutant. Altogether, these results suggested that exomer might have two functions with respect to Ena1: first, exomer could enhance expression of Ena1 and, second, exomer might be required for polarized Ena1 plasma membrane localization. Both possibilities are not mutually exclusive. The polarization coefficient would indicate that exomer is required for Ena1 polarized localization, but we cannot rule out a transcriptional contribution.

Therefore, we investigated Ena1-GFP localization independently of its transcriptional regulation using the inducible promotor tetO
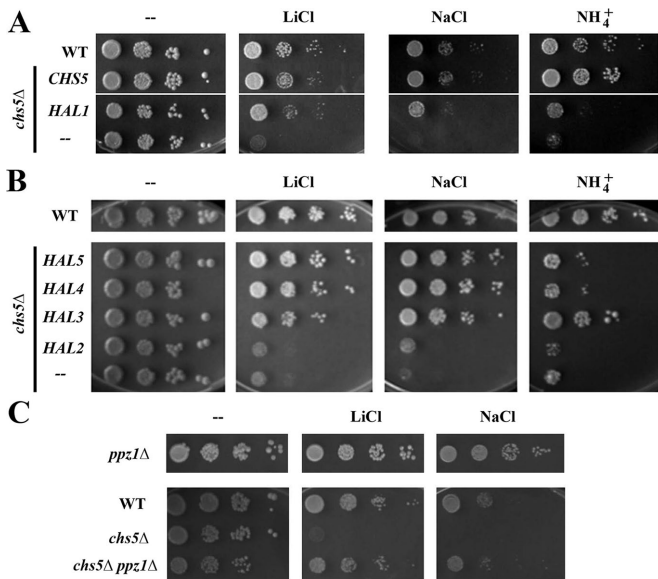
FIGURE 3: Multicopy suppression analysis by *HAL* genes. (A) Growth of the wild-type and *chs5Δ* strains transformed with the indicated genes on SD media supplemented with the indicated compounds. (B) Drop assays of *chs5Δ* transformed with different *HAL* genes. Wild-type strain is used as the control. In all cases, *HAL* genes were overexpressed from multicopy plasmids (YEp351 or Yep352). Cells were grown in selective SD to ~2 × 10⁷ cells/ml media and serially diluted before spotting onto YPD plates containing either 0.2 M LiCl, 0.2 M (NH₄)₂SO₄, or 1 M NaCl. Plates were incubated 2–3 d at 30°C. (C) Deletion of *PPZ1* rescues the *chs5Δ* growth defect on LiCl and NaCl plates. Drop assay with different strains. Plates were incubated 2–3 d at 30°C.

(Marques *et al.*, 2015). In this system, Ena1-GFP expression was regulated in a doxycycline (dox) concentration-dependent manner, in which 10 µg/ml abolished Ena1-GFP expression and 0.1 µg/ml allowed some expression (Figure 5D). After 2 h of induction, levels of Ena1-GFP were similar in wild type and the *chs5Δ* mutant, inde-

pendent of the dox concentration (Figure 5D). We then determined Ena1-GFP localization after 2 h of growth in dox at concentrations of 10 and 0.1 µg/ml. At high dox, Ena1-GFP is barely visible and the localization of the protein was similar in wild-type and *chs5Δ* strains (Figure 5E). NaCl stress-induced Ena1-GFP polarization was less efficient in *chs5Δ* cells, with a level that reached only ~50% when compared with wild type (Figure 5, E and F). Moreover, at 0.1 µg/ml dox in the absence of saline stress, Ena1-GFP was observed neatly polarized in the wild-type cells (40.3±7.8%), while *chs5Δ* cells showed a more uniform staining with less than 10% of the cells displaying a polarized Ena1-GFP distribution. Cationic treatment increased polarization not only in wild type but also in the *chs5Δ* mutant, which maintained reduced polarization levels of Ena1-GFP compared with the control (Figure 5F). Similar results were obtained when we determined the polarization coefficient for Ena1-GFP under a variety of conditions and in different strains (Supplemental Figure S3C). Altogether our results demonstrate the direct involvement of exomer in Ena1 polarization. It is worth noting that degradation of Ena1-GFP in the vacuole appeared minimal and indistinguishable between wild-type and *chs5Δ* mutants (see images and Supplemental Figure S2C), arguing against a direct effect of exomer on Ena1 recycling.

All previously described exomer cargoes show a strong polarized distribution (Figure 6), a hallmark that is also shared by Ena1. Therefore, we addressed whether the localization of other polarized proteins was affected in *chs5Δ*. However, neither the localization of the SNARE Snc1 nor of the osmosensor Sho1 was altered under those conditions (Figure 6). Another common feature shared between Chs3 and Ena1 is that they both require Sro7 for proper localization (Wadskog *et al.*, 2006; Zanolari *et al.*, 2011). Therefore, we tested whether other Sro7-dependent plasma membrane proteins (Forsmark *et al.*, 2011) would also be exomer-dependent cargoes. The hexose transporter Hxt7 and the glycerol symporter Stl1 localized indistinguishably in wild type and *chs5Δ*. Apparently exomer is involved in the polarized delivery of a restricted number of TM proteins. However, contrary to the other exomer cargoes described to date, Ena1 is still able to efficiently reach the PM in the absence of a functional exomer.
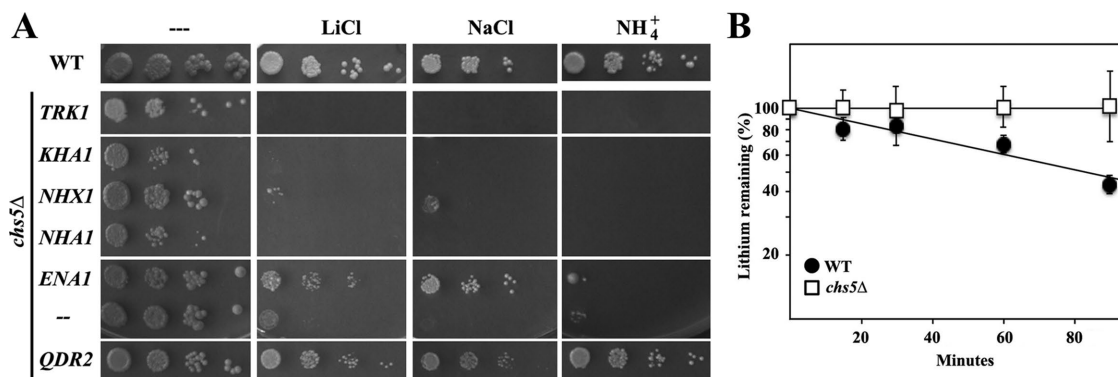
FIGURE 4: Effect of the overexpression of different ionic transporters on the *chs5Δ* phenotypes. (A) *chs5Δ* cells were transformed with the indicated genes expressed from multicopy plasmids, grown on selective SD media to 2 × 10⁷ cells/ml, serially diluted and spotted onto the plates as in Figure 3. Growth was scored after 2 d at 30°C. Note the reduced sensitivity of the *chs5Δ* mutant to LiCl and NaCl, but not to (NH₄)₂SO₄, after *ENA1* overexpression, while high levels of *QDR2* improved growth on the three media. (B) Li⁺ extrusion in the indicated strains. Cells were preloaded with Li⁺ and transferred to fresh media. Cells were collected at the indicated times, and the internal amounts of Li⁺ were measured by atomic absorption. Data are presented as the percentage of the original values of the strain at 0 time. The results are the average of three independent cultures. See *Materials and Methods* for details. Note the limited extrusion capacity of the *chs5Δ* mutant.
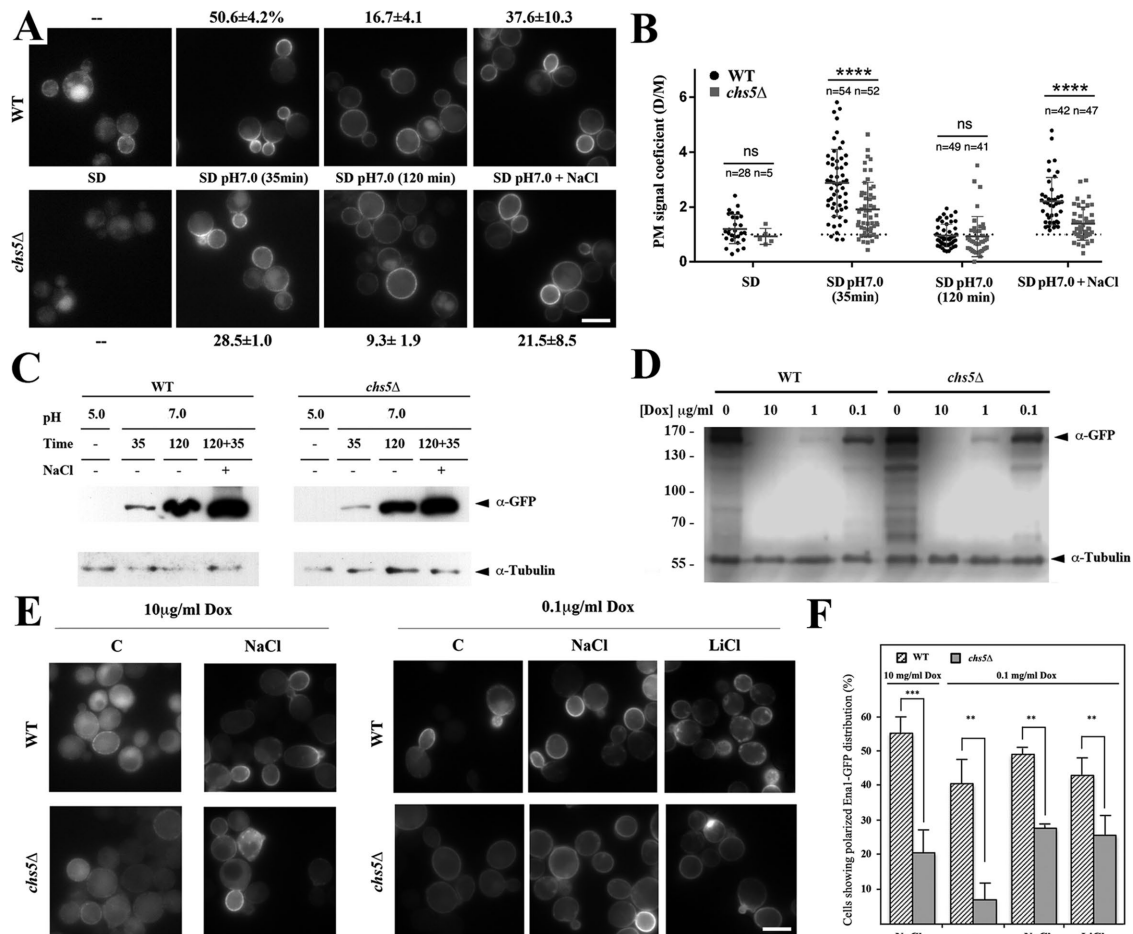
FIGURE 5: Assessing the role of exomer on Ena1 function. (A) Localization of a chromosomally tagged version of Ena1-GFP in wild type and *chs5Δ*. Cells were grown on selective SD media to logarithmic phase and then incubated under the indicated conditions. The percentage of cells showing polarized distribution of the fluorescence signal associated with Ena1-GFP is given as average values with standard deviations. (B) Polarization coefficients for any measured cell (*n* = number of cells) in the experiment described in A. See *Materials and Methods* for details. (C) Ena1-GFP levels before and after alkalinization of SD media under the same experimental conditions as in A. (D) Levels of Ena1-GFP expressed from the tetO promoter. Cells were grown in the presence of 10 mg/ml dox and transferred for 2 h to fresh media supplemented with the indicated concentrations of the drug. (E) Ena1-GFP was visualized by fluorescence microscopy after growth on the indicated dox concentration for 2 h. Cation treatment was performed for additional 30 min. (F) Levels of Ena1-GFP polarization in the same experiment. The results are the average of at least three independent experiments counting at least 50 cells in each experiment. Note the higher polarization of Ena1-GFP in wild type in all conditions tested. See also Supplemental Figure S3 for a complementary quantitative analysis on Ena1-GFP polarization.

Lack of exomer strongly reduces Rim101 processing and activation at neutral and alkaline pH

So far, we demonstrated that Ena1-GFP localization is altered in *chs5Δ* cells. However, we also observed a reduction of Ena1 protein levels in the exomer mutant, which is not explained by vacuolar degradation. Under the same conditions, the cellular concentration of Qdr2 was increased (Figure 2A), suggesting an opposite transcriptional control of the levels of Ena1 and Qdr2. Indeed, loss of the transcription factor Rim101 produced a similar deregulation effect on the expression of both *ENA1* and *QDR2* genes (Lamb and Mitchell, 2003). Rim101 positively regulates transcription of alkaline-expressed genes such as Ena1 (Lamb and Mitchell, 2003). To explore whether Chs5 impacts the transcriptional response triggered by Rim101, we first compared the sensitivity to alkali ions of the single and double mutants (Figure 7A). As expected, *chs5Δ* and *rim101Δ* shared sensitivities toward alkali metals and alkaline

growth medium, with *rim101Δ* being somewhat more sensitive. Combining both mutations exacerbated the phenotypes, indicating that they may act in parallel pathways. However, this result by itself does not exclude a potentially negative effect of *chs5Δ* on Rim101 function. Rim101 is activated at neutral-alkaline pH through proteolytic cleavage by the sequential action of several components of the RIM101 signaling pathway (Lamb *et al.*, 2001). Therefore, we assessed Rim101 processing in *chs5Δ*. In wild type, Rim101 is cleaved and thereby activated when the pH in the growth medium is raised from 5 to 7 (Figure 7B). In contrast, proteolytic activation of Rim101 was abolished in *chs5Δ* (Figure 7B). Thus, the *chs5Δ* cation sensitivity can be partially explained by the inability to activate the Rim101-dependent response.

Next, we addressed the mechanism by which lack of Chs5 abolishes Rim101 activation. The arrestin Rim8 is recruited to the PM by the pH sensor Rim21 (Herrador *et al.*, 2015), where it becomes
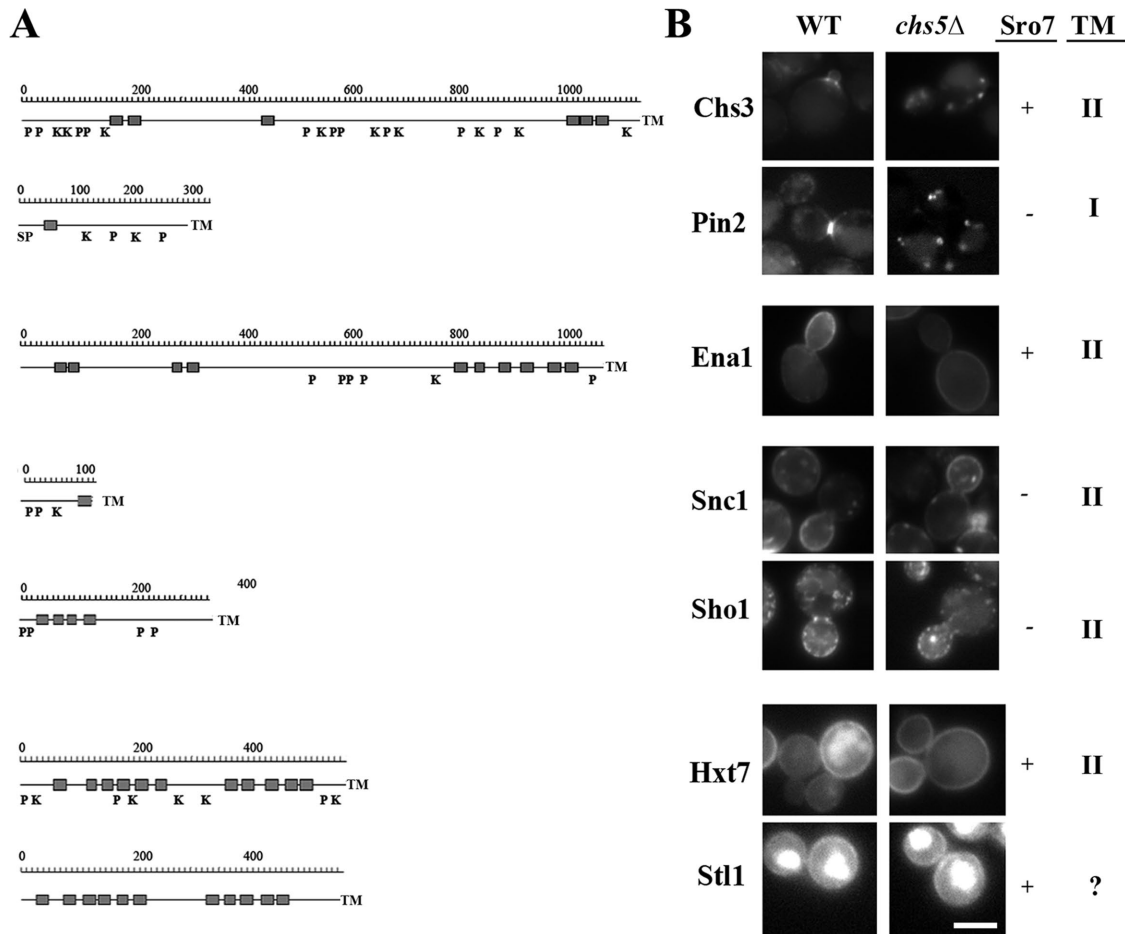
FIGURE 6: Localization of PM proteins in *chs5Δ* mutant cells. (A) Hydrophobic profiles of the indicated proteins showing predicted transmembrane domains (gray squares) and signal peptide (SP) sequences. The postranslational modifications that have been experimentally described for these proteins are also indicated: P (phosphorylation) and K (ubiquitination). The profiles are drawn to approximate scale. (B) Representative images showing protein localization in wild-type and *chs5Δ* cells. The dependence of these proteins on Sro7 that has been previously described (Forsmark *et al.*, 2011) is indicated, as well as their predicted nature as Type I or II TM proteins. Chs3 and Pin2 have been described as bona fide exomer cargoes. Note how Ena1 polarization, but not PM arrival, is defective in the *chs5Δ* mutant. The absence of exomer did not affect the localization of the other proteins. See Figure 2A for additional images on other permeases.

ubiquitinated under alkaline conditions (Herranz *et al.*, 2005). In turn, ubiquitinated Rim8 recruits the ESCRT-I protein Vps23 to the PM (Herrador *et al.*, 2010; Galindo *et al.*, 2012), which triggers the recruitment of the processing machinery consisting of Rim20 and the protease Rim13 (Obara and Kihara, 2014) (reviewed in Peñalva *et al.* [2014]). Unfortunately, the fluorescent signals of Rim8-RFP and Vps23-GFP were too weak for proper analysis. We therefore determined the localization of Rim13 and Rim20 at acidic and alkaline pH. The number of Rim13/20 foci after alkalinization of the media increased significantly in wild type but remained essentially unchanged in the *chs5Δ* mutant (Figure 7C and Supplemental Figure S4), explaining the poor processing of Rim101 in this mutant at pH 8.0. If our interpretation of these results was correct, then we would expect an alleviation of *chs5Δ* phenotypes on restoring Rim101 processing. To test this hypothesis, we expressed a constitutively processed form of Rim101 (Rim101^C [Lamb *et al.*, 2001]) that mimics the effect of alkali signaling. Under those conditions, we observed increased basal levels of Ena1-GFP in both wild-type and *chs5Δ* cells (Figure 7D). However, Rim101^C had only

a modest effect on the *chs5Δ* phenotypes (Figure 7E), whereas it suppressed more efficiently the phenotypes of the *rim13Δ* and *rim20Δ* mutants (Figure 7E), which are likewise defective in Rim101 processing (Hayashi *et al.*, 2005). These results indicate that while the defective processing of Rim101 could contribute to the phenotypes of the *chs5Δ* mutant, it is probably not the major cause for the sensitivity of exomer mutant to cations. Therefore, Chs5 must be involved in at least one other independent pathway regulating the response to cations.

Exomer is required for efficient Rim21 plasma membrane localization

These results, however, raised another question as to why exomer would be involved in Rim101 processing. One possibility is that exomer could be involved in the recruitment of Rim20/13 to the cortical foci, or, potentially, the transport of PM sensors like Rim21, which are part of the RIM101 signaling pathway might be perturbed. To distinguish between these possibilities, we addressed the behavior of Rim21 in the *chs5Δ* mutant. Rim21 levels were not affected at
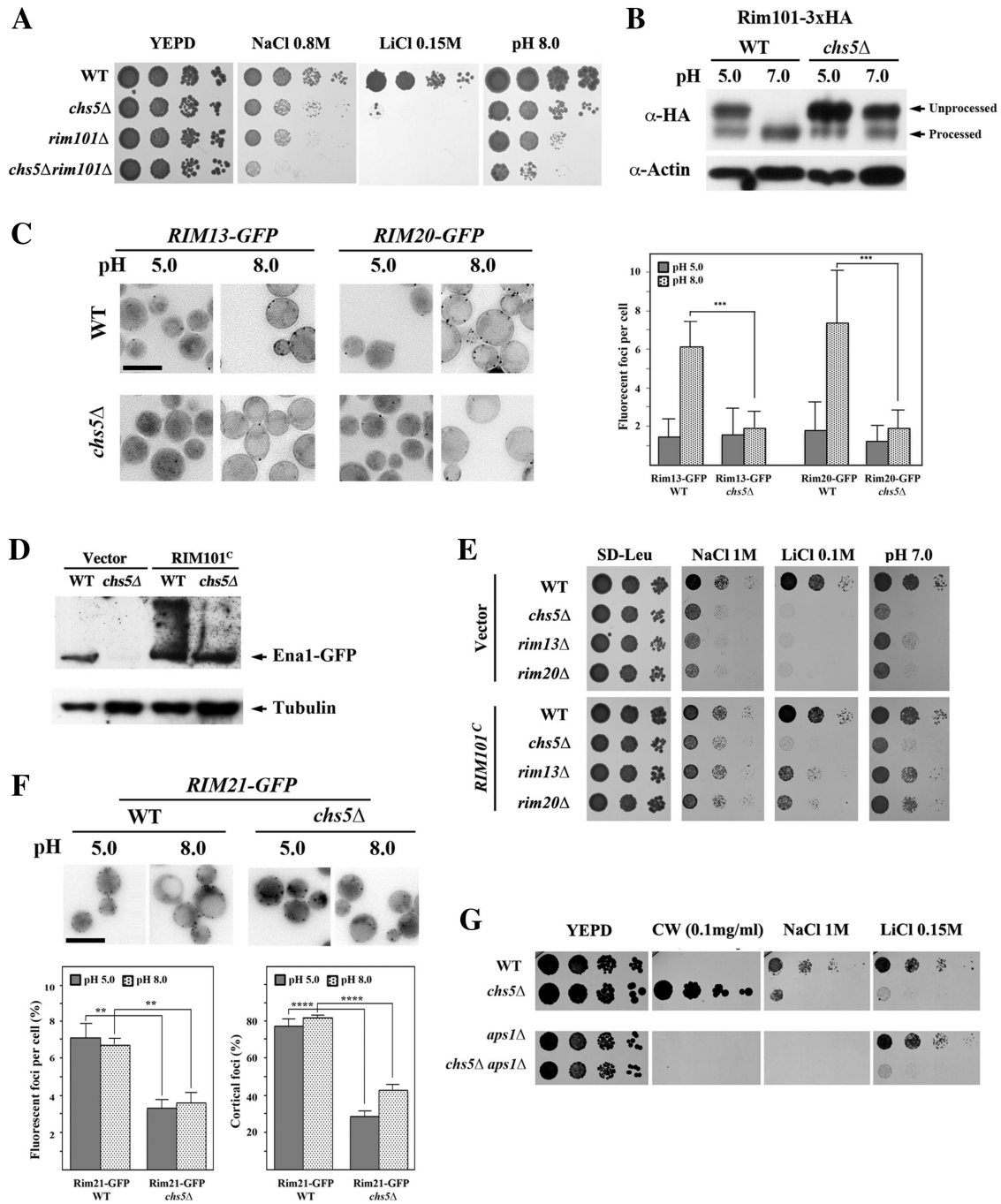
FIGURE 7: Defective RIM101 signaling in the exomer mutant. (A) Comparative phenotypes of *rim101Δ* and *chs5Δ* mutants. Note the similar phenotypes observed and the additive effect of both mutations. (B) Immunoblot of Rim101 proteolytic processing at the indicated pHs. Cells contain a modified version of Rim101 with an internal 3xHA tag. Note the absence of processing in the *chs5Δ* mutant compared with the control. (C) Visualization of processing spots using yeast cells containing chromosomally tagged versions of Rim13 and Rim20 proteins. Note the increasing numbers of spots for both proteins after alkalinization of the media for 1 h in wild type, which is absent in the *chs5Δ* mutant. Right panel shows the quantitative results for this experiment, which are the average of three independent experiments. (D) Levels of Ena1-GFP from its endogenous locus after expression of the constitutively processed Rim101[C] from the pRS315 plasmid. Cells were grown O/N in selective SD media and refreshed in YEPD media for 2 h. (E) Drop assay of strains transformed with the constitutively expressed form of Rim101 (pRS315::*RIM101*[C]) on the indicated media. Note the moderate improvement of growth promoted by Rim101[C] in the *chs5Δ* mutant under all conditions tested. (F) Rim21-x2GFP localization in the indicated strains/conditions. Note the lower cortical localization of the protein in the *chs5Δ* mutant independently of the media pH. The quantitative results are the average of at least three independent experiments counting at least 120 cells in each experiment. (G) Phenotypes of the indicated mutants in different media. Note that the absence of Aps1 restores wild-type calcofluor sensitivity of the *chs5Δ* mutant but not its growth on Na^{+} or Li^{+} plates.

the different pHs in *chs5Δ* compared with wild type (see Supplemental Figure S4A). In contrast, Rim21-2xGFP fluorescent foci differed significantly between strains. Rim21-2xGFP was mostly localized as discrete spots in the cell periphery in wild type at either pH 5.0 or pH 8.0 (Figure 7F). By contrast, the number of Rim21-2xGFP spots in the *chs5Δ* mutant was reduced, and the spots were distributed throughout the cell volume in the *chs5Δ* mutants, showing a reduced association with the cell periphery (Figure 7F). Treatment with latrunculin A (LatA) to block endocytosis did not improve the numbers of cortical foci in the *chs5Δ* mutant (Supplemental Figure S4B), and these foci partially colocalized with the TGN marker Sec7 (Supplemental Figure S4C). These results suggest that Rim21 is at least partially retained at the TGN in the *chs5Δ* mutant, suggesting Rim21 localization might be dependent on exomer. Yet, all exomer-dependent cargoes described so far regain PM localization on AP-1 deletion, which was not the case for Rim21. The deletion of *APS1* has a minor effect on the cortical localization of Rim21-2xGFP foci (Supplemental Figure S4D). Nevertheless, *chs5Δ aps1Δ* mutant cells were still as sensitive as *chs5Δ* for growth on alkali metal-containing medium (Figure 7G), and Rim101 remained essentially unprocessed at alkaline pH in the double mutant (see Supplemental Figure S4E). Our results thus indicate that exomer is required for the efficient localization of the Rim21 sensor at the PM, which is essential for proper signaling by the RIM101 pathway.
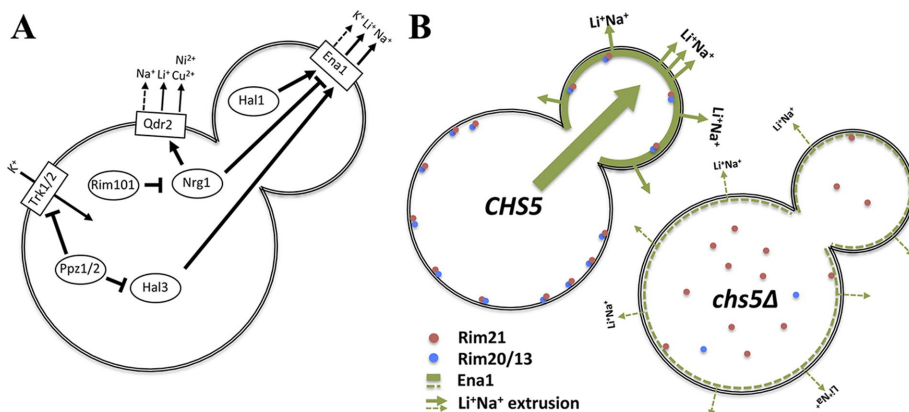
DISCUSSION

Ena1, a potential new exomer cargo with distinct properties

Exomer is required for the delivery of several proteins to the PM, including Chs3, Fus1, and Pin2. However, none of these cargoes can be linked to the sensitivity to cationic compounds of exomer-deficient strains. In contrast, theses sensitivities are observed in mutants of cation transporters such as Trk1/2 or Ena1-4. In addition, our multicopy suppression analysis revealed the ability of several *HAL* genes to suppress the sensitivity of the *chs5Δ* mutant toward alkali metal cations. Deletion of Ppz1/2 phosphatases, which act as negative regulators of halotolerance, also reduced the sensitivity of exomer mutants to Na⁺ or Li⁺ (see Figure 8A). Moreover, exomer mutants displayed a reduction in K⁺ influx resulting in reduced intracellular K⁺ levels. Consistently, high K⁺ concentrations suppressed the *chs5Δ* sensitivity to hygromycin (Figure 1B). However, external K⁺ had a minor effect on Na⁺/Li⁺ sensitivity, arguing against a direct defect in K⁺ transport as the major reason

for exomer sensitivity to alkali metal cations. Accordingly, overexpression of the K⁺ transporter Trk1 did not rescue the sensitivity of the *chs5Δ* to alkali metal cations. In contrast, overexpression of the efflux pumps Qdr2 and Ena1 effectively rescued this phenotype. Because overexpression of Qdr2 also alleviated the NH₄⁺ sensitivity of exomer deficiency, it is likely that the Qdr2 effect is a consequence of its activity as a general cation transporter with low specificity (Ríos *et al.*, 2013).

Our data are most consistent with the model in which the Na⁺/Li⁺ sensitivity of *chs5Δ* is caused by the reduced activity of Ena1 at the plasma membrane. It is tempting to speculate that Ena1 may be a new exomer cargo because of its structural similarity to Chs3. However, Ena1 efficiently reaches the PM in the absence of exomer. Nevertheless, the polarized delivery of Ena1 is significantly reduced in the *chs5Δ* mutants (Figure 5, Supplemental Figure S3, and Figure 8B). We hypothesize that for Ena1 to act as a detoxifier it needs to be localized to the bud in order to protect the growing bud. The bud is particularly sensitive to any insult—such as Li⁺/Na⁺ stress—because the cell wall in this area is less rigid and less complex than in the mother. As a consequence, the effects of the alkali metals in cell integrity may be more severe in the bud than in the mother. It is also conceivable that Ena1 localization distinctly shields the bud from damage, considering that it is destined to become the young daughter after cell division. There is also a transcriptional component as Ena1 levels are lower in the *chs5Δ* mutant. Therefore, the combination of the reduced levels of the protein together with its altered distribution can explain the sensitivity of *chs5Δ* to alkali metal cations.

The role of exomer in Ena1 polarization as well as in the polarization of previously described bona fide cargos, such as Fus1, Chs3, or Pin2, caused us to speculate that exomer may have a general role in the polarized delivery of TM proteins. However, neither Sho1 nor Snc1, as examples of other highly polarized TM proteins, showed altered localization in the *chs5Δ* mutant. Moreover, the dependence of both Chs3 and Ena1 on Sro7 on their transit to the PM did not seem to be mechanistically relevant because other TM proteins also transported through Sro7, such as Hxt7 or Stl1, showed normal localization in the exomer-deficient mutants. Furthermore, exomer function may be even more general. For example, Skg6, also localized in a polarized manner, can bind to the exomer complex in vivo and in vitro but is not dependent on exomer for polarized localization in rich medium (Ritz *et al.*, 2014).

Hence, what would be the common characteristics for these proteins? There is no common trait in terms of amino acid sequence, topology, functional domains, and number of transmembrane domains. It appears as if there were several types of proteins whose traffic depends on exomer and that in a general sense they could be considered exomer cargoes. Bona fide cargoes are strictly dependent on exomer such as Chs3, Fus1, and Pin2. They require constant endocytosis and recycling through the TGN for their polar PM localization. Conversely, other types of cargoes are not strictly dependent on exomer. They can use alternative pathways and do not require constant endocytosis and recycling through the TGN; examples are Skg6 (Ritz *et al.*, 2014) and the here described Ena1. Our data point toward a more general role

FIGURE 8: Scheme for exomer's role on Ena1 function. (A) Simplified scheme of the control of alkali metal cation transport across the PM in *S. cerevisiae*. (B) Exomer controls alkali metal cation sensitivity by directly controlling Ena1 polarization and indirectly controlling Ena1 levels through the activation of the RIM101 signaling pathway.

for exomer in polarized secretion, which is compatible with its previously described role as a dedicated cargo adaptor (Bonifacino, 2014; Paczkowski *et al.*, 2015). In this more general scenario for exomer function, we expect an increase in the numbers of proteins dependent on exomer for polarized PM localization to be described in the future.

Expanding exomer functionality at the TGN

In addition to functioning as a cargo adaptor, exomer may have additional roles. Ena1 protein levels were reduced in the *chs5Δ* mutant, which was accompanied by an increase of Qdr2 protein expression. These effects were a direct consequence of a deficient RIM101 signaling pathway caused by the poor processing of Rim101 protein in the *chs5Δ* mutant. Accordingly, *chs5Δ* and *rim101Δ* mutants share multiple phenotypes (Figure 7A). Moreover, expression of a constitutively processed form of Rim101 partially alleviated the Na^+/Li^+ sensitivity of the *chs5Δ* mutant.

Our results unambiguously showed a clear defect in the recruitment of the RIM101 processing machinery (see Figure 8B for a schematic summary), which may help to explain the improper processing of Rim101. In the *chs5Δ* mutant, the alkaline pH sensor Rim21 did not efficiently reach the PM, impeding the Rim20 and Rim13 recruitment to the PM after alkalinization of the media. This failure prevents Rim101 proteolytic processing by the Rim13 protease and a reduction in RIM101 signaling, causing decreased Ena1 and increased Qdr2 levels. The simplest explanation for Rim21 mislocalization is that either Rim21 itself or one of its interaction partners, Dfg16 and Rim9, is an exomer cargo. However, deletion of AP-1 complex did not significantly improve Rim21 PM localization and Rim101 processing in the *chs5Δ* mutant. Furthermore, all exomer cargoes are localized in a polarized manner while the Rim21 complex does not have a polar distribution and may not require AP-1 recycling. Therefore, the possibility that at least one component of the Rim101 signaling complex could be an exomer cargo, although unlikely, remains open.

Alternatively, but not mutually exclusively, the defective recruitment of processing foci could be due to an aberrant TGN compartment organization in exomer mutants. Consistent with this possibility, *chs5Δ*, like multiple endosomal mutants, is sensitive to hygromycin and rapamycin (Figure 1 and Parsons *et al.* [2004] and Fell *et al.* [2011]). Moreover, *chs5Δ* genetically interacts with several *vps* mutants (Costanzo *et al.*, 2010), including *vps27Δ*, *vps24Δ* and several components of the retromer and CORVET complexes, highlighting an altered function of the late endosomal compartment in the absence of exomer. This function is fully in line with the previously proposed role of exomer at the TGN/EE boundary where, in addition to its role as cargo adaptor, it may amplify the membrane remodeling activity of the Arf1 GTPase. Impaired Arf1 GTPase activity has an important impact on the membranes of the TGN/EE boundary (Yahara *et al.*, 2001) and explains the phenotypes described. The expansion of the Golgi membrane in the *arf1-18* mutant (Yahara *et al.*, 2001) is reminiscent to the Golgi structure observed in an exomer/AP-1 double mutant in *Schizosaccharomyces pombe* (Hoya *et al.*, 2017), consistent with a role of Arf1 in exomer and AP-1-dependent transport.

In summary, our work describes new biological roles for the exomer complex at the TGN, expanding its function as a direct adaptor for a restricted number of bona fide cargoes to a more general one involved in the polarized secretion of multiple proteins. Both roles are equally compatible with the function of organizing a platform for loading cargo at the TGN, which would contribute to the proper traffic of many other proteins through the different endosomal compartments. This function would be similar to the one of Sec16, for example, in organizing transitional ER exit sites (Kung *et al.*, 2012). Obviously, this also raises the possibility that this organizing function, apart from being a cargo adaptor, might be evolutionary conserved from the simplest form of exomer present in most fungi.

MATERIALS AND METHODS
Yeast strains construction
The yeasts strains used throughout this work were made in the W303 or YPH499 genetic backgrounds as indicated in Table 1. Gene deletions were made using the gene replacement technique with different deletion cassettes based on *natMX4*, *kanMX4*, and *hphNT1* resistance (Goldstein and McCusker, 1999). Proteins were tagged chromosomally at their C-terminus with 3xHA or GFP, employing integrative cassettes amplified from pFA6a-3HA-hphMx6 or pFA6a-GFP-hphMx6, respectively (Sato *et al.*, 2005). *RIM21-2xGFP* construction was made using a specific set of primers and a plasmid with the cassette *2xGFP::kanMX4*. Whenever possible, GFP-tagged proteins were tested for functionality. In particular, chromosomally tagged Ena1-GFP was shown to be functional by testing the sensitivity of the corresponding strains to several stresses (Supplemental Figure S1A). Functionality of the pCM262::*ENA1-GFP* [tetO7-*ENA1-GFP::URA3*] construct has been previously reported (Marques *et al.*, 2015). The effect of different mutations on the localization of the tagged proteins were tested by deleting the corresponding genes on the strain contained the tagged protein to avoid the variability caused by potentially different versions of the tagged protein. The effects of the different mutations were always tested in two independent clones.

General methods for yeast handling have been previously described (Rose *et al.*, 1990). In brief, yeasts were transformed using the standard lithium acetate/polyethylene glycol procedure.

The plasmids used in this work are described in Table 2.

Media and growth assays
Yeast cells were grown at 28°C or 30°C in YEPD (1% Bacto yeast extract, 2% peptone, and 2% glucose) or in SD medium (2% glucose, 0.7% Difco yeast nitrogen base without amino acids) supplemented with the appropriate amino acids. Medium was supplemented before pouring with different compounds at the concentration indicated for each experiment. In most cases, NaCl was added between 0.7 and 1.0 M, LiCl from 0.1 to 0.2 M, NH_4Cl from 0.1 to 0.2 M, and Calcofluor White from 0.01 to 0.3 mg/ml. Hygromycin was used between 40 and 100 µg/ml, and, when required, the pH of the media was adjusted with 50 mM phosphate buffer at pH 5.0 and 7.0 and Tris-HCl buffer to pH 8.0.

Drop tests
For assessment of the growth phenotypes, fresh cells of each tested strain were resuspended in water and adjusted to 1.0 OD_{600}. Tenfold serial dilutions were prepared, and drops were spotted onto appropriate YEPD or SD agar plates supplemented as indicated in the text. Plates were incubated at 28°C for 2–5 d.

Gradient plates were prepared by successive pouring of two layers of media with different compositions. The first layer (containing the tested compound) was poured into a moderately inclined square Petri dish. After solidification, the plate was placed into a flat position, and the second layer (with the same composition, only without the inhibitory compounds) was poured on top (Maresova and Sychrova, 2005). In these experiments, the same dilution of the culture (OD_{600} = 0.1) was spotted along the plate.

Strain	Genotype	Origin/Reference
CRM67	W303, mat a, (leu2-3,112 trp1-1 can1-100 ura3-1 ade2-1 his3-11,15)	Lab collection
CRM2268	W303, mat a, *chs5Δ::natMx4*	Lab collection
CRM2688	W303, mat a, *trk1Δ::LEU2 trk2Δ::HIS3*	Madrid *et al.* (1998)
CRM2689	W303, mat a, *ena1-4Δ::HIS3*	Yenush *et al.* (2002)
CRM1590	W303, mat a, *chs3Δ::natMx4*	Lab collection
CRM3056	W303, mat a, *rim101Δ::kanMx4*	This study
CRM2888	W303, mat a, *NHA1-GFP::hphNT1*	This study
CRM2896	W303, mat a, *chs5Δ::natMx4 NHA1-GFP::hphNT1*	This study
CRM1278	W303, mat a, *chs3Δ::URA3 chs5Δ::natMx4*	Lab collection
CRM3119	W303, mat a, *HXT7-GFP::hphNT1*	This study
CRM3121	W303, mat a, *chs5Δ::natMx4 HXT7-GFP::hphNT1*	This study
CRM3117	W303, mat a, *STL1-GFP::hphNT1*	This study
CRM3121	W303, mat a, *chs5Δ::natMx4 STL1-GFP::hphNT1*	This study
CRM3058	W303, mat a, *chs5Δ::natMx4 rim101Δ:: kanMx4*	This study
CRM3085	W303, mat a, *RIM101-3xHA::LEU2*	This study
CRM3086	W303, mat a, *chs5Δ::natMx4 RIM101-3xHA::LEU2*	This study
CRM3133	W303, mat a, *RIM21-2xGFP::kanMx4*	This study
CRM3153	W303, mat a, *RIM21-2xGFP::kanMx4 chs5Δ::natMx4*	This study
CRM3094	W303, mat a, *RIM13-GFP::kanMx4*	This study
CRM3096	W303, mat a, *chs5Δ::natMx4 RIM13-GFP::kanMx4*	This study
CRM3098	W303, mat a, *RIM20-GFP::kanMx4*	This study
CRM3100	W303, mat a, *chs5Δ::natMx4 RIM20-GFP::kanMx4*	This study
CRM3155	W303, mat a, *aps1Δ::kanMx4*	This study
CRM3157	W303, mat a, *chs5Δ::natMx4 aps1Δ::kanMx4*	This study
CRM2406	W303, mat a, *PIN2-GFP::hphNT1*	This study
CRM2507	W303, mat a, *chs5Δ::natMx4 PIN2-GFP::hphNT1*	This study
CRM3198	W303, mat a, *RIM101-3xHA::LEU2 aps1Δ::hphNT1*	This study
CRM3191	W303, mat a, *chs5Δ::natMx4 RIM101-3xHA::LEU2 aps1Δ::hphNT1*	This study
YAS2157	YPH499, *QDR2-GFP::TRP1*	This study
YAS2158	YPH499, *QDR2-GFP::TRP1 chs5Δ::LEU2*	This study
YAS2202	YPH499, *ENA1-GFP::TRP1*	This study
YAS2241	YPH499, *ENA1-GFP::TRP1 chs5Δ::LEU2*	This study
CRM3159	YPH499, *ENA1-GFP::TRP1 chs5Δ::natMx4*	This study
YAS563-16a	YPH499, *bch1Δ::HIS5 (S. pombe) bch2Δ::KAN (Tn 903) bud7Δ::LEU2 (K. lactis) chs6Δ::URA3 (K. lactis)*	Trautwein *et al.* (2006)
YAS563-5a	YPH499, *bch1Δ::HIS5 (S. pombe)*	Trautwein *et al.* (2006)
YAS1974	YPH499, *ppz1Δ::HIS5 (S. pombe)*	This study
YAS1975	YPH499, *ppz1Δ::HIS5 (S. pombe) chs5Δ::LEU2*	This study
YPH499	Mat a, *ura3-52 lys2-801 ade2-101 trp1-Δ63 his3-Δ200 leu2-Δ1*	Spang lab
YAS431	YPH499, *chs5Δ::LEU2*	Spang lab
CRM3273	W303, mat a, *RIM21-2xGFP::kanMx4 SEC7-mRuby2::URA3*	This study
CRM3274	W303, mat a, *RIM21-2xGFP::kanMx4 SEC7-mRuby2::URA3 chs5Δ::natMX4*	This study
FCM603	W303, mat a, *RIM13::natMx4*	Lab collection
CRM3381	W303, mat a, *vps27Δ::kanMx4 chs5Δ::natMX4*	This study
CRM3382	W303, mat a, *vps27Δ::kanMx4*	This study

TABLE 1: Yeast strains used.

Plasmid	Genotype	Origin/Reference
CRM2684	pRS414::*TRK1-GFP*	Yenush *et al.* (2005)
CRM2686	pCM262::*ENA1-GFP* [tetO7-ENA1-GFP::URA3]	Marques *et al.* (2015)
CRM1598	pR315::*CHS3-GFP*	Sacristan *et al.* (2013)
CRM1715	pRS315::*GFP-SNC1*	Spang lab
CRM1855	pRS416::*SHO1-GFP*	F. Posas, Universidad Pompeu Fabra, Spain
CRM3075	pKR41::*RIM101-3xHA::LEU2*	Rothfels *et al.* (2005)
FCM129	pWL86 [pRS314::*RIM101C*^{531}]	Li and Mitchell (1997)
FCM591	pRS315:: *RIM101C*^{531}	Lab collection
CRM2071	pYM38::*2xGFP-kanMx4*	R. Wedlich-Söldner, University of Muenster, Germany
RS702	yEP351::*HAL1*	Rios *et al.* (1997)
JRM5	yEP351::*HAL2*	Murguia *et al.* (1996)
RS1068	yEP351::*HAL3*	Ferrando *et al.* (1995)
PM73	yEP351::*HAL4*	Mulet *et al.* (1999)
PM89	yEP351::*HAL5*	Mulet *et al.* (1999)
pRG296-2	pGN621::*TRK1*	Gaber *et al.* (1988)
JM1	yEP351::*KHA1*	This study
JM3	yEP351::*NHX1*	This study
JM4	yEP351::*NHA1*	This study
YAS1254	YEp24::*ENA1*	Ferrando *et al.* (1995)
PM71	yEP351::*QDR2*	Ríos *et al.* (2013)

TABLE 2: Plasmids used.

Multicopy suppressor screen

One hundred nanograms of a Yep24 genomic plasmid library (Carlson and Botstein, 1982) was transformed into *chs5Δ* cells using the LiAc method. For this experiment, aliquots were plated out on either Hartwell s Complete minus uracil (HC-URA) or YEPD 0.2 M LiCl plates and incubated at 30°C. The next day, colonies from HC-URA plates were replica plated onto YEPD 0.2 M LiCl plates and YEPD 0.2 M LiCl-derived colonies onto HC-URA. Colonies from both regimes were replica plated onto HC-URA and YEPD 0.2 M LiCl plates. Colonies that grew on both plates were expanded, and the plasmids were isolated and sequenced.

K$^+$ content of cells and Rb$^+$/Li$^+$ transport experiments

The time course of Rb$^+$ uptake of actively growing cells was studied in YEPD media as described (Mulet and Serrano, 2002). When the OD$_{600}$ of the culture reached values of 0.3, RbCl (50 mM) was added to the medium (time zero), and cell samples were removed at various times afterward for the intracellular determination of Rb$^+$. Intracellular K$^+$ was determined in logarithmically growing cells in YEPD.

For the determination of intracellular levels of Rb$^+$/K$^+$ cells were grown as indicated above, collected by centrifugation, and washed twice with 10 ml of an ice-cold 20 mM MgCl$_2$ solution. The cell pellets were finally resuspended in 0.5 ml of the same 20 mM MgCl$_2$ solution. Ions were extracted by heating the cells for 15 min at 95°C. After centrifugation, aliquots of the supernatant were analyzed with an atomic absorption spectrometer (SensAA) in flame emission mode.

For the Li$^+$ extrusion experiments, cells were grown to an OD$_{600}$ of 0.6, collected by centrifugation and transferred to fresh YEPD containing 0.2 M LiCl. After 4 h incubation, cells were centrifuged, washed twice with a 20 mM MgCl$_2$ solution, and transferred to fresh YEPD. Aliquots were taken at the indicated times. Sample treatment and lithium determination were performed as for the Rb$^+$/K$^+$ experiments.

Fluorescence microscopy

Yeast cells expressing GFP-tagged proteins were grown to early logarithmic phase in SD medium supplemented with 0.2% adenine. Living cells were visualized directly by fluorescence microscopy.

Most of the images were obtained using a Nikon 90i epifluorescence microscope (100× objective, NA: 1.45), equipped with a Hamamatsu ORCA ER digital camera, and by using a 49002 ET-GFP (FITC/Cy2) and 49005 ET-DsRed (TRITC/Cy3) filters (Chroma Technology Corp). The images were then processed using the ImageJ software (NIH) and mounted with Adobe Photoshop CS5 (San José, CA) software. All images shown in each series were acquired under identical conditions and processed in parallel to preserve the relative intensities of fluorescence for comparative purposes. In all figures, the white scale bar represents 5 μm.

Where appropriate, image measurements were statistically analyzed using the *t* test for unpaired data. Analyses were performed using the GraphPad Prism (GraphPad Software, La Jolla, CA) software. Significantly different values ($p < 0.05$, $p < 0.01$, and $p < 0.001$) are indicated (*, **, ***).

Quantification of the Ena1-GFP polarization

To obtain an unbiased measurement of the cellular polarization of Ena1-GFP, we determined the daughter/mother plasma membrane signal coefficient (polarization coefficient) at every single cell. Intensities were measured on raw images with FIJI software (ImageJ) by drawing a line along the cell contour (*Freehand Line, 8 Line Width*)

and acquiring the average intensity value (*Analyze/measure*); an intensity value was obtained for every mother and daughter cell (the bud). Measurements were only performed at budded cells following the schemes represented (Supplemental Figure S2A) depending on the size of the bud. The background average intensity in the cell proximity for every single cell was subtracted. After the background subtraction, the daughter/mother polarization coefficient was calculated for every cell, $C = D/M$.

Colocalization of Rim21-2xGFP with Sec7-mR2 positive structures

Quantification was performed in FIJI software (ImageJ) as follows. First, both green and red channels were prefiltered with a dedicated macro to eliminate most of the background. Then a threshold was manually adjusted for Sec7-mR2 images before loading Sec7-mR2 regions of interest (ROIs) at ROI Manager (*Image/Adjust/Threshold, Analyze/Analyze Particles, Size 6-1000, Circularity 0-1*). After that, the Sec7-mR2 ROIs were overlapped to the pre-filtered Rim21-2xGFP images and the colocalization of Rim21 particles with Sec7 ROIs was manually accounted with the cell counter tool (*Plugins/Analyze/Cell Counter*). Note that Rim21-2xGFP ROIs were not acquired because Rim21-2xGFP signal was too dim to obtain an accurate threshold.

Protein extracts and immunoblotting

Total cell lysates were prepared by resuspending cells obtained from the 30-ml logarithmic cultures in 150 µl of lysis buffer (50 mM Tris-HCl, pH 8, 0.1% Triton, 150 mM NaCl) containing 1× protease inhibitor cocktail (1 mM PMSF, 1 µg ml^{-1} aprotinin, 1 µg ml^{-1} leupeptin, 1 µg ml^{-1} pepstatin A). Cells were disrupted using glass beads (0.45 mm, SIGMA) during three pulses of 15 s each with an intensity of 5.5 units in a Fast prep (FP120, BIO101). Cell debris was eliminated by centrifugation (5 min, $10,000 \times g$, 4°C) and the resultant supernatant was boiled for 5 min with 4× sample buffer (0.2 M Tris-HCl pH 6.8, 4% SDS, 40% glycerol, 4% β-mercaptoethanol); 100 µg of protein per sample was used.

For visualizing Ena1-GFP and Rim21-2xGFP in Western blot experiments, the trichloroacetic acid (TCA) protocol was used. To do this, the same OD$_{600}$ of cells from the logarithmic cultures was processed for each sample, and the entire procedure was carried out on ice until the boiling step. Cells were centrifuged, resuspended in 20% TCA, and frozen for at least 3 h. The samples were then thawed and the centrifuged cells were disrupted in 1.5-ml tubes with 100 µl of 20% TCA and glass beads (0.45 mm; Sigma) during three pulses of 15 s with an intensity of 5.5 in a Fast prep (FP120, BIO101). Extracts were transferred to new tubes, and 5% TCA was added to the extracts up to final TCA concentration of ~10%. Precipitated proteins were then collected by centrifugation at $900 \times g$ for 10 min and the supernatant was completely discarded. Then 50 µl of 2× sample buffer was added (100 mM Tris-HCl, pH 6.8, 4% SDS, 20% glycerol, 25 mM dithiothreitol (DTT), and traces of bromophenol blue) and vortexed, and an additional 50 µl of 2 M Tris-HCl, pH 7.5, was added. The extracts were boiled for 5 min and centrifuged for 5 min at $15,000 \times g$. The supernatant was collected, and 15 µl was used for Western blot analysis.

Both types of extracts were separated on 7.5% SDS–PAGE (6.5% for Rim21-2xGFP) and transferred onto PVDF membranes (Trilla *et al.*, 1999). The membranes were blocked with skimmed milk and incubated with the corresponding antibodies: anti-GFP JL-8 monoclonal antibody (Living colors; Clontech), anti-HA 12CA5 (Roche), anti-tubulin (T5162; Sigma), depending on the experiments. Blots were developed using the ECL kit (Advansta).

For determining Rim101 expression, cells growing logarithmically in selective SD media were transferred at an OD$_{600}$ of 0.4 into fresh SD media (pH 5.0 and 7.0) and incubated for an additional 3 h and then processed as indicated above.

REFERENCES

Ariño J, Ramos J, Sychrová H (2010). Alkali metal cation transport and homeostasis in yeasts. Microbiol Mol Biol Rev 74, 95–120.

Bard F, Malhotra V (2006). The formation of TGN-to-plasma-membrane transport carriers. Annu Rev Cell Dev Biol 22, 439–455.

Barfield RM, Fromme JC, Schekman R (2009). The exomer coat complex transports Fus1p to the plasma membrane via a novel plasma membrane sorting signal in yeast. Mol Biol Cell 20, 4985–4996.

Bonifacino JS (2014). Adaptor proteins involved in polarized sorting. J Cell Biol 204, 7–17.

Bonifacino JS, Glick BS (2004). The mechanisms of vesicle budding and fusion. Cell 116, 153–166.

Bonifacino JS, Lippincott-Schwartz J (2003). Coat proteins: shaping membrane transport. Nat Rev Mol Cell Biol 4, 409–414.

Carlson M, Botstein D (1982). Two differentially regulated mRNAs with different 5' ends encode secreted and intracellular forms of yeast invertase. Cell 28, 145–154.

Costanzo M, Baryshnikova A, Bellay J, Kim Y, Spear ED, Sevier CS, Ding H, Koh JL, Toufighi K, Mostafavi S, *et al.* (2010). The genetic landscape of a cell. Science 327, 425–431.

De Matteis MA, Luini A (2008). Exiting the Golgi complex. Nat Rev Mol Cell Biol 9, 273–284.

de Nadal E, Clotet J, Posas F, Serrano R, Gomez N, Ariño J (1998). The yeast halotolerance determinant Hal3p is an inhibitory subunit of the Ppz1p Ser/Thr protein phosphatase. Proc Natl Acad Sci USA 95, 7357–7362.

Drubin DG, Nelson WJ (1996). Origins of cell polarity. Cell 84, 335–344.

Fell GL, Munson AM, Croston MA, Rosenwald AG (2011). Identification of yeast genes involved in k homeostasis: loss of membrane traffic genes affects k uptake. G3 (Bethesda) 1, 43–56.

Ferrando A, Kron SJ, Rios G, Fink GR, Serrano R (1995). Regulation of cation transport in Saccharomyces cerevisiae by the salt tolerance gene HAL3. Mol Cell Biol 15, 5470–5481.

Forsmark A, Rossi G, Wadskog I, Brennwald P, Warringer J, Adler L (2011). Quantitative proteomics of yeast post-Golgi vesicles reveals a discriminating role for Sro7p in protein secretion. Traffic 12, 740–753.

Gaber RF, Styles CA, Fink GR (1988). TRK1 encodes a plasma membrane protein required for high-affinity potassium transport in Saccharomyces cerevisiae. Mol Cell Biol 8, 2848–2859.

Galindo A, Calcagno-Pizarelli AM, Arst HN, MÁ Peñalva (2012). An ordered pathway for the assembly of fungal ESCRT-containing ambient pH signalling complexes at the plasma membrane. J Cell Sci 124, 1784–1795.

Goldstein AL, McCusker JH (1999). Three new dominant drug resistance cassettes for gene disruption in Saccharomyces cerevisiae. Yeast 15, 1541–1553.

Hayashi M, Fukuzawa T, Sorimachi H, Maeda T (2005). Constitutive activation of the pH-responsive Rim101 pathway in yeast mutants defective in late steps of the MVB/ESCRT pathway. Mol Cell Biol 25, 9478–9490.

Herrador A, Herranz S, Lara D, Vincent O (2010). Recruitment of the ESCRT machinery to a putative seven-transmembrane-domain receptor is mediated by an arrestin-related protein. Mol Cell Biol 30, 897–907.

Herrador A, Livas D, Soletto L, Becuwe M, Léon S, Vincent O (2015). Casein kinase 1 controls the activation threshold of an α-arrestin by multisite phosphorylation of the interdomain hinge. Mol Biol Cell 26, 2128–2138.

Herranz S, Rodríguez JM, Bussink HJ, Sánchez-Ferrero JC, Arst HNJ, Peñalva MA, Vincent O (2005). Arrestin-related proteins mediate pH signaling in fungi. Proc Natl Acad Sci USA 102, 12141–12146.

Hoya M, Yanguas F, Moro S, Prescianotto-Baschong C, Doncel C, de León N, Curto MÁ, Spang A, Valdivieso MH (2017). Traffic through the trans-Golgi network and the endosomal system requires collaboration between exomer and clathrin adaptors in fission yeast. Genetics 205, 673–690.

Huranova M, Muruganandam G, Weiss M, Spang A (2016). Dynamic assembly of the exomer secretory vesicle cargo adaptor subunits. EMBO Rep 17, 202–219.

Kung LF, Pagant S, Futai E, D'Arcangelo JG, Buchanan R, Dittmar JC, Reid RJ, Rothstein R, Hamamoto S, Snapp EL, et al. (2012). Sec24p and Sec16p cooperate to regulate the GTP cycle of the COPII coat. EMBO J 31, 1014–1027.

Lamb TM, Mitchell AP (2003). The transcription factor Rim101p governs ion tolerance and cell differentiation by direct repression of the regulatory genes NRG1 and SMP1 in Saccharomyces cerevisiae. Mol Cell Biol 23, 677–686.

Lamb TM, Xu W, Diamond A, Mitchell AP (2001). Alkaline response genes of Saccharomyces cerevisiae and their relationship to the RIM101 pathway. J Biol Chem 276, 1850–1856.

Li W, Mitchell AP (1997). Proteolytic activation of Rim1p, a positive regulator of yeast sporulation and invasive growth. Genetics 145, 63–73.

Madrid R, Gómez MJ, Ramos J, Rodríguez-Navarro A (1998). Ectopic potassium uptake in trk1 trk2 mutants of Saccharomyces cerevisiae correlates with a highly hyperpolarized membrane potential. J Biol Chem 273, 14838–14844.

Maresova L, Sychrova H (2005). Physiological characterization of Saccharomyces cerevisiae kha1 deletion mutants. Mol Microbiol 55, 588–600.

Marques MC, Zamarbide-Fores S, Pedelini L, Llopis-Torregrosa V, Yenush L (2015). A functional Rim101 complex is required for proper accumulation of the Ena1 Na+-ATPase protein in response to salt stress in Saccharomyces cerevisiae. FEMS Yeast Res 15, fov017.

Mulet JM, Leube MP, Kron SJ, Rios G, Fink GR, Serrano R (1999). A novel mechanism of ion homeostasis and salt tolerance in yeast: the Hal4 and Hal5 protein kinases modulate the Trk1-Trk2 potassium transporter. Mol Cell Biol 19, 3328–3337.

Mulet JM, Serrano R (2002). Simultaneous determination of potassium and rubidium content in yeast. Yeast 19, 1295–1298.

Murguia JR, Belles JM, Serrano R (1996). The yeast HAL2 nucleotidase is an in vivo target of salt toxicity. J Biol Chem 271, 29029–29033.

Obara K, Kihara A (2014). Signaling events of the Rim101 pathway occur at the plasma membrane in a ubiquitination-dependent manner. Mol Cell Biol 34, 3525–3535.

Paczkowski JE, Fromme JC (2014). Structural basis for membrane binding and remodeling by the exomer secretory vesicle cargo adaptor. Dev Cell 30, 610–624.

Paczkowski JE, Richardson BC, Fromme JC (2015). Cargo adaptors: structures illuminate mechanisms regulating vesicle biogenesis. Trends Cell Biol 25, 408–416.

Paczkowski JE, Richardson BC, Strassner AM, Fromme JC (2012). The exomer cargo adaptor structure reveals a novel GTPase-binding domain. EMBO J 31, 4191–4203.

Parsons AB, Brost RL, Ding H, Li Z, Zhang C, Sheikh B, Brown GW, Kane PM, Hughes TR, Boone C (2004). Integration of chemical-genetic and genetic interaction data links bioactive compounds to cellular target pathways. Nat Biotechnol 22, 62–69.

Peñalva MA, Lucena-Agell D, Arst HNJ (2014). Liaison alcaline: Pals entice non-endosomal ESCRTs to the plasma membrane for pH signaling. Curr Opin Microbiol 22, 49–59.

Perlin DS, Brown CL, Haber JE (1988). Membrane potential defect in hygromycin B-resistant pma1 mutants of Saccharomyces cerevisiae. J Biol Chem 263, 18118–18122.

Ríos G, Cabedo M, Rull B, Yenush L, Serrano R, Mulet JM (2013). Role of the yeast multidrug transporter Qdr2 in cation homeostasis and the oxidative stress response. FEMS Yeast Res 13, 97–106.

Rios G, Ferrando A, Serrano R (1997). Mechanisms of salt tolerance conferred by overexpression of the HAL1 gene in Saccharomyces cerevisiae. Yeast 13, 515–528.

Ritz AM, Trautwein M, Grassinger F, Spang A (2014). The prion-like domain in the exomer-dependent cargo Pin2 serves as a trans-Golgi retention motif. Cell Rep 10, 249–260.

Rockenbauch U, Ritz AM, Sacristan C, Roncero C, Spang A (2012). The complex interactions of Chs5p, the ChAPs, and the cargo Chs3p. Mol Biol Cell 23, 4404–44015.

Roncero C (2002). The genetic complexity of chitin synthesis in fungi. Curr Genet 41, 367–378.

Roncero C, Sanchez-Diaz A, Valdivieso MH (2016). Chitin synthesis and fungal morphogenesis. In: The Mycota III: Biochemistry and Molecular Biology, ed. D Hoffmeister, Berlin: Springer, 167–190.

Rose MD, Wisnton F, Hieter P (1990). Methods in Yeast Genetics: A Laboratory Course Manual, New York: Cold Spring Harbor Laboratory Press.

Rothfels K, Tanny JC, Molnar E, Friesen H, Commisso C, Segall J (2005). Components of the ESCRT pathway, DFG16, and YGR122w are required for Rim101 to act as a corepressor with Nrg1 at the negative regulatory element of the DIT1 gene of Saccharomyces cerevisiae. Mol Cell Biol 25, 6772–6788.

Sacristan C, Manzano-Lopez J, Reyes A, Spang A, Muniz M, Roncero C (2013). Dimerization of the chitin synthase Chs3 is monitored at the Golgi and affects its endocytic recycling. Mol Microbiol 90, 252–266.

Santos B, Snyder M (1997). Targeting of chitin synthase 3 to polarized growth sites in yeast requires Chs5p and Myo2p. J Cell Biol 136, 95–110.

Sato M, Dhut S, Toda T (2005). New drug-resistant cassettes for gene disruption and epitope tagging in Schizosaccharomyces pombe. Yeast 22, 582–591.

Schekman R, Orci L (1996). Coat proteins and vesicle budding. Science 271, 1526–1533.

Sopko R, Huang D, Preston N, Chua G, Papp B, Kafadar K, Snyder M, Oliver SG, Cyert M, Hughes TR, et al. (2006). Mapping pathways and phenotypes by systematic gene overexpression. Mol Cell 21, 319–330.

Spang A (2008). The life cycle of a transport vesicle. Cell Mol Life Sci 65, 2781–2789.

Starr TL, Pagant S, Wang CW, Schekman R (2012). Sorting signals that mediate traffic of chitin synthase III between the TGN/endosomes and to the plasma membrane in yeast. PLoS One 7, e46386.

Trautwein M, Schindler C, Gauss R, Dengjel J, Hartmann E, Spang A (2006). Arf1p, Chs5p and the ChAPs are required for export of specialized cargo from the Golgi. EMBO J 25, 943–954.

Trilla JA, Duran A, Roncero C (1999). Chs7p, a new protein involved in the control of protein export from the endoplasmic reticulum that is specifically engaged in the regulation of chitin synthesis in Saccharomyces cerevisiae. J Cell Biol 145, 1153–1163.

Valdivia RH, Baggot D, Chuang JS, Schekman R (2002). The yeast Clathrin adaptor protein complex 1 is required for the efficeint retention of a subset of late Golgi membrane proteins. Dev Cell 2, 283–294.

Wadskog I, Forsmark A, Rossi G, Konopka C, Oyen M, Goksör M, Ronne H, Brennwald P, Adler L (2006). The yeast tumor suppressor homologue Sro7p is required for targeting of the sodium pumping ATPase to the cell surface. Mol Biol Cell 17, 4988–5003.

Wang CW, Hamamoto S, Orci L, Schekman R (2006). Exomer: a coat complex for transport of select membrane proteins from the trans-Golgi network to the plasma membrane in yeast. J Cell Biol 174, 973–983.

Weiskoff AM, Fromme JC (2014). Distinct N-terminal regions of the exomer secretory vesicle cargo Chs3 regulate its trafficking itinerary. Front Cell Dev Biol 2, 47.

Yahara N, Ueda T, Sato K, Nakano A (2001). Multiple roles of Arf1 GTPase in the yeast exocytic and endocytic pathways. Mol Biol Cell 12, 221–238.

Yenush L, Merchan S, Holmes J, Serrano R (2005). pH-Responsive, post-translational regulation of the Trk1 potassium transporter by the type 1-related Ppz1 phosphatase. Mol Cell Biol 25, 8683–8692.

Yenush L, Mulet JM, Ariño J, Serrano R (2002). The Ppz protein phosphatases are key regulators of K+ and pH homeostasis: implications for salt tolerance, cell wall integrity and cell cycle progression. EMBO J 21, 920–929.

Zanolari B, Rockenbauch U, Trautwein M, Clay L, Barral Y, Spang A (2011). Transport to the plasma membrane is regulated differently early and late in the cell cycle in Saccharomyces cerevisiae. J Cell Sci 124, 1055–1066.